Int J Adv Manuf Technol (2013) 67:701–718
DOI 10.1007/s00170-012-4516-2

ORIGINAL ARTICLE

Tool wear prediction models during end milling of glass fibre-reinforced polymer composites

A. I. Azmi · R. J. T. Lin · D. Bhattacharyya

Received: 28 February 2012 / Accepted: 11 September 2012 / Published online: 29 September 2012

Abstract Composite products are often subjected to secondary machining processes as integral part of component manufacture. However, rapid tool wear becomes the limiting factor in maintaining consistent machining quality of the composite materials. Hence, this study demonstrates the development of an indirect approach in predicting and monitoring the wear on carbide tool during end milling using multiple regression analysis (MRA) and neuro-fuzzy modelling. Although the results have indicated that acceptable predictive capability can be well achieved using MRA, the application of neuro-fuzzy yields a significant improvement in the prediction accuracy. It is apparent that the accuracies are pronounced as a result of nonlinear membership function and hybrid learning algorithms. Using the developed models, a timely decision for tool re-conditioning or tool replacement can be achieved effectively.

Keywords Tool wear prediction · End milling · GFRP composites · Regression analysis · Neuro-fuzzy modelling

A. I. Azmi (✉) · R. J. T. Lin · D. Bhattacharyya
Centre for Advanced Composite Materials (CACM), Department of Mechanical Engineering, The University of Auckland, Private Bag 92019, Auckland, New Zealand
e-mail: aazm007@aucklanduni.ac.nz

R. J. T. Lin
e-mail: rj.lin@auckland.ac.nz

D. Bhattacharyya
e-mail: d.bhattacharyya@auckland.ac.nz

A. I. Azmi
School of Manufacturing Engineering, Universiti Malaysia Perlis, Ulu Pauh Campus,
02600, Pauh, Perlis, Malaysia
e-mail: azwaniskandar@unimap.edu.my

1 Background

Advanced composite materials such as fibre-reinforced polymer (FRP) composites have been regularly designed and manufactured for various structural and functional applications. Their appealing properties can also be deliberately tailored in improving fire resistance, thermal and electric insulation, as well as the sound absorption. These make them desirable for non-structural products, in areas, such as acoustic or panel wall applications. In common practise, composite products are endeavoured to be manufactured to the near-net shapes. Nonetheless, finishing steps that involve machining are inevitably essential to meet the final dimensional and functional requirements of the composite products. In spite of this, cutting mechanisms of FRP composites are very different from conventional metallic material. The cutting processes are characterised by the combinations of material fracturing, shearing, buckling and bending, and interlaminar failures with little plastic deformation owing to the laminate structure, inherent anisotropic, and brittleness of fibre reinforcements [1–3]. Moreover, it is literally known that fibre orientations, types of polymer matrix, as well as the bonding strength between fibres and the matrix material distinguish the machinability of FRP composites from that of homogeneous metals [4–6]. Among different machinability characteristics, quality consistencies of machined surface and tool life expectancy have been found to be critically linked to the fibre structure within the FRP composites [7, 8]. The damage susceptibility FRP composites can significantly impede the consistency of machining quality on the workpiece, whereas its abrasiveness inflicts rapid wear on the cutting tools. It is well understood that mechanical abrasion on the flank face of the cutting tool characterises the primary tool wear mechanism when machining FRP composites [4, 8]. In addition, low thermal conductivities of both matrix material and the glass fibres may result in a higher temperature in the

cutting zone. This can also be accounted for the increase in wear of the cutting tool. Very often, inadequate sharpness of the cutting tools increases the likelihood of inducing surface damage to composite materials. Poor surface qualities of the composite products degrade their in-service or mechanical performance and under the worst circumstances, get them rejected prior to the final usage.

A review of literature reveals that a number of experimental efforts have been carried out to elucidate and improve the machinability of FRP composites under different machining processes [8–13]. Yet, very little has considered the milling operation. This could mainly be attributed to the complexity associated with the cutting actions in milling operation. Notably, due to multiple cutting edges, the cutting mechanisms change with different fibre orientations and/or architecture. The intermittent cutting mechanisms of milling operation also lead to variations of chip sizes, contact stresses and cyclic temperatures. Under certain machining conditions, the fluctuated loadings on the cutting tool may easily change the cutting mechanisms from that of continuous machining. Hence, the physical and mathematical descriptions for end milling of FRP composites still remain a challenge. In addition to the previous study on optimising machining parameters using Taguchi methodology [14], other results with regard to improvement of surface quality and reduction of delamination damage on the machined composites have been reported recently in Refs. [15–17]. However, the various aspects of developing general and accurate tool wear prediction models for end milling of glass fibre-reinforced polymer (GFRP) composites are still hardly mentioned. For any machining operation, continuous monitoring of the tool wear is imperative for determination of a suitable time for tool replacement or reconditioning in order to alleviate any adverse effects of the worn tool on the machined surface. The common practice for monitoring the tool condition is by directly measuring the size of wear lands on tool flank or rake faces. However, the drawbacks of this method are: (1) it is time consuming, and (2) the machining operation has to be interrupted in order to determine the extent of tool wear. In contrast, an indirect approach of tool condition monitoring that involves measurements of machining signals, which can be correlated to the tool wear, offers a more practical solution for industrial applications. Indeed, previous studies on different machinability domains have shown that the growth of tool wear not only depends on the machining conditions but also on the forces generated during machining [18–22]. Hence, this paper presents the development of generalised tool wear prediction models for end milling of GFRP composites using measured machining forces under a broad range of machining parameters.

Two tool wear modelling approaches are proposed, namely the multiple regression analysis (MRA) and the adaptive network-based fuzzy inference systems (ANFIS) or simply known as neuro-fuzzy. In the former, general empirical models are derived to establish mathematical equations or constitutive relationships between tool wear and the machining forces, whereas, the latter is used to further improve the predictive capability. In spite of the more implicit expression, the use of artificial intelligence (AI) or soft computing techniques, such as neural network and fuzzy logic have been found to be more suitable to solve complex, nonlinear and imprecise relationships that exist among experimental variables. One of the main attractions of the soft computing approach is that it is not necessary to postulate a complex mathematical model beforehand, in order to describe experimental relationships.

Principally, a constitutive relationship of experimental parameters can be 'learned' by a neural network model through adequate training of experimental data. On the other hand, a fuzzy logic model constructs the input–output mapping according to human thinking characteristics or decision rules using the stipulated input–output data pairs. Hitherto, a number of research works have reported successful applications of artificial neural networks (ANN), particularly for modelling machinability output characteristics, such as surface roughness, machining forces and tool wear in metal cutting [17–23]. The research studies on modelling of machinability characteristics have reported the successful applications of radial basis function and the multi-layer perceptron (MLP) neural networks for composite materials [17, 19, 30]. Until recently, the development of tool wear predictive model for condition monitoring through fuzzy logic modelling coupled with neural network training, while end milling GFRP composites has not been attempted. One of the advantages of ANFIS modelling is the use of hybrid learning procedures (from neural network training) and fuzzy reasoning (from fuzzy logic) for predicting the consequent (effect) parameters due to the premise (cause) parameters [27–29].

2 Experimental procedure

2.1 Sample manufacturing

Composite testing specimens for the end milling experiments were GFRP plates, made of uni-directional E-glass fibre-reinforced thermosetting epoxy resin. They were fabricated using vacuum assisted resin infusion. Sixteen layers of E-glass fibre mats (EU450-1270 supplied by SP High Modulus (NZ)) of 300×300 mm were laid up dry on a flat glass panel to create a preform. This preform is then properly sealed by vacuum bagging and arrangement of peel ply and distribution media. The use of distribution media is to facilitate the uniform flow of resin during filling, whereas the peel ply allows easy removal of distribution media once the composite panels/plates are fully cured. Subsequently, epoxy resin (Nuplex R300) and hardener (Nuplex R310) mixed in a

4:1 ratio were infused into the E-glass preform under a vacuum pressure of approximately 10 mbar (1 kPa). The infused panel was left to cure for more than 12 h under room temperature, and further post cured in an oven at 60–70 °C. The cured panels were cut, using a water-cooled diamond saw, into size of 200×135×6 mm, for the machining experiments. Cap screw holes were drilled into the sample plates for secured mounting onto the Kistler® 9265B piezoelectric milling dynamometer. The fibre volume fraction, v_f, was regularly monitored according to ASTM D3171-09 to ensure the consistency of the manufactured part quality. The average value of v_f for the manufactured sample plates was 0.52.

2.2 Experimental matrix

In order to establish a complete tool wear response, a series of experiments were carried out over a wide spectrum of end milling parameters, which were based on preliminary experiments as well as results from previously published work [14]. These parameters were selected such that they covered the practical range of industrial applications and were within the limit of the CNC machine. The summary of the machining parameters employed in this study is given in Table 1. The axial depth of cut was kept constant at 2 mm, as this parameter was found previously to be less important towards tool wear or tool life [14]. This depth of cut was chosen for a decent material removal rate to maintain uniform growth of flank wear and to facilitate the morphological study of the machined surface through scanning electron microscopy.

2.3 Milling experiment and data acquisition equipment

The end milling tests were carried out on a Centroid 1050A CNC machine centre (8,000 rpm maximum spindle speed and 28 kW power). As the tests were conducted under dry conditions, a vacuum cleaner was used to handle the hazardous chips and to minimise the chip interference on the cutting edge, which could lead to a local heat accumulation in the cutting zone [30]. For the cutting tool selection, despite the commercially available PCD and diamond-coated tools for machining 'difficult to cut' material such as composite materials, carbide tools are still widely used in the industry as well as in the research related to composites machining [15, 16, 30, 31, 34]. Hence, uncoated tungsten carbide end mill cutter of 12 mm diameter (supplied by SGS Tools, Inc) was selected as the cutting tool in this study. To further evaluate the effects of fibre orientation on machining performance, cutting tests were performed using the same sets of machining parameters in two directions: (1) 0° when the table or tool feed was along the fibre orientation and (2) 90°, across the fibre orientation (Fig. 1). These two fibre orientations represent the extreme cases, as far as the tool wear is concerned, based on preliminary experiments conducted previously. Kistler® 9265B piezoelectric milling dynamometer with Kistler® 5001 charge amplifier was used to monitor the feed force, F_x, and the cutting force, F_y, generated after each end milling pass (Fig. 1). The machining force signals were acquired through a PC with LabVIEW data acquisition system. Replication tests under selected conditions were performed to ensure repeatability of the experiments, with deviations to be within ±5–10 %. Depending on the machining conditions and tool wear rate, the machining process was interrupted at predetermined intervals in order to measure the extent of tool wear on each cutting flute. The optical study of the tool wear was performed under the Leica MZ16 optical stereo microscope.

Within the range of testing parameters, abrasive wear was found to be the dominant tool wear mechanism. This was observed on the flank face of each cutting flute. Digital camera attached to the microscope was used to capture images of flank wear at different machining times. From the images captured, flank wear height was measured using the UTHSCSA Image Tool® software. The extent of flank wear was determined based on average of three measurements of flank wear heights on each of the cutting flutes. Upon reaching an average flank wear value of 0.3 mm, the experiment was stopped, and the tool useful life based on total machining time was determined for subsequent analysis.

Table 1 Machining conditions

Machining conditions	Values
Spindle speed, N	3,000; 4,000; 5,000; 6,000 RPM
Effective linear cutting speed, s	110, 150, 190, 230 m/min
Feed rate, f	0.16, 0.24, 0.32 mm/rev
Fibre orientation/ angle, A	0°, 90°

3 Modelling of tool wear

3.1 Multiple regression analysis

MRA is a widely used statistical modelling technique to establish empirical models or mathematical relationships between a dependent variable and the independent variables. In the present work, the dependency of the output variable, Y, is considered by a power law function:

$$Y = Cs^{a}f^{\beta}F^{\gamma}A^{\zeta} \tag{1}$$

where C is the empirical constant, s, f, F, A are the input parameters and α, β, γ and ζ are the corresponding exponents of the empirical model. The exponent for each independent

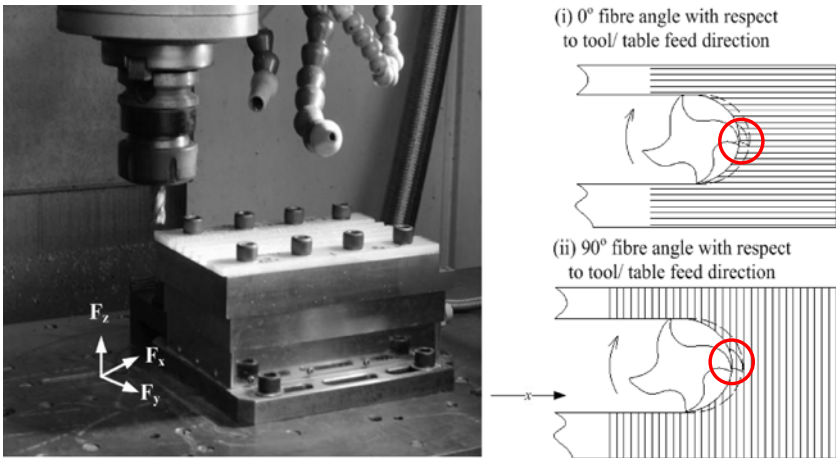

Fig. 1 Set-up for the end milling experiments showing x as the table feed direction and the different fibre orientations

variable determines the effect it has on the dependent variable. The adequacy of the developed empirical model can be verified using the coefficient of correlation, R^2, which measures the variability in the data accounted for by the model. R^2 will have a value of between 0 and 1, where a value of 1 would mean perfect correlation while 0 means no correlation exists between dependent and independent variables.

3.2 Fuzzy logic or fuzzy inference system

Fuzzy logic or fuzzy inference system (FIS) has been one of the popular and effective soft computing methods used to model control and automation systems. On the basis of its multidisciplinary nature, FIS is also particularly attractive in other engineering applications. This includes the modelling of highly nonlinear input and output experimental relationships in machining operations [21]. Typically, FIS employs a human reasoning or human structured knowledge in the form of fuzzy rules (rather than using mathematical models) to match a given input into an output. The FIS model normally consists of three components, which are the data base, the rule base and the fuzzy output. The database defines fuzzy membership functions (MFs) to be used in the FIS, whereas, the rule base contains a selection of fuzzy rules and an inference system to carry out fuzzy reasoning of the input MFs to produce fuzzy outputs. Finally, defuzzification of the fuzzy output gives the final crisp value of the FIS. The primary working mechanism of an FIS is through the construction of a set of fuzzy rules (in the form of *IF–THEN* statements) which will then be evaluated in parallel using fuzzy operators, such as *AND*, *OR* and *NOT* to determine the functional relationships.

3.2.1 Architecture of the adaptive network-based fuzzy inference system

ANFIS (also known as Neuro Fuzzy) is an advanced FIS with learning capability of a neural network. This feature distinctively differentiates it from the traditional FIS, as the neural network training algorithm enables the change in the FIS structure and its parameters. Due to this fact, fine tuning of the predicted output would be possible [21]. Additionally, the application of fuzzy inferencing allows better interpretability of the neural network while maintaining the accuracy of the input–output matching [21]. This reduces large computational efforts which would typically be required in the traditional neural network algorithm, such as the multi-layer perceptron neural network. Similar to that of any neural network model, working principles of ANFIS is also based on its architecture [21]. It provides the mapping of input–output dataset through combination of 'learning' and 'fine-tuning' procedures of the neural network and fuzzy inferencing. Figure 2 exhibits a simple ANFIS architecture consisting of two inputs (x and y), each with two MFs, a fuzzy rule base (number of rules, R) and a single output, f. The network implements the first-order (linear function) Takagi–Sugeno-type fuzzy reasoning for learning and fine tuning. Examples of the first-order Takagi–Sugeno fuzzy rules are as follow:

Rule 1: IF x is A_1 AND y is B_1 THEN z is $f_1(x,y)$
where $f_1=p_1x+q_1y+r_1$
Rule 2: IF x is A_2 AND y is B_2 THEN z is $f_2(x,y)$
where $f_2=p_2x+q_2y+r_2$

The aforesaid fuzzy rules can be depicted as in Fig. 2a, where x and y represent the inputs, z is the output, and A_1, A_2, B_1, B_2 are the nonlinear parameters or fuzzy sets (representing the linguistic variables such as *SMALL*, *MEDIUM* and *HIGH*). The p_1, p_2, q_1, q_2, r_1 and r_2 are linear parameters for the Takagi–Sugeno first-order models, f_1 and f_2. As depicted in Fig. 2b, the ANFIS architecture comprises five distinct layers of feed-forward neural network. Typically, the layers are characterised by the operations that they perform, namely: (1) fuzzification; (2) rule base; (3) normalising; (4) defuzzification and (5) output of layer 1 to 5. Furthermore, each layer of the architecture is represented by different node functions, which can be in the form of adaptive nodes

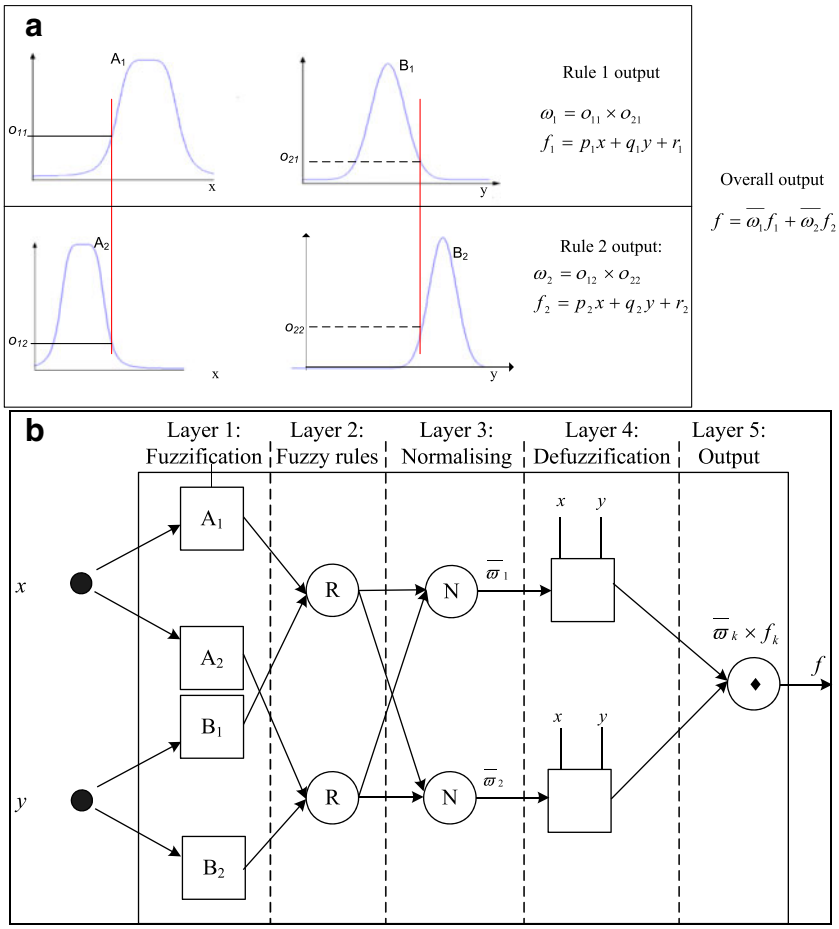

Fig. 2 **a** First-order Takagi–Sugeno fuzzy inference model **b** architecture of Adaptive Network-Based Fuzzy Inference System (ANFIS)

(denoted by squares) and fixed nodes (denoted by circles). The parameter sets are adjustable in the adaptive nodes and vice versa for the fixed nodes. During fuzzy inferencing, output signals from each layer are manipulated by the node functions so as to provide the input signals for the subsequent layer.

3.2.2 Processing of node functions in ANFIS architecture

The processing of node functions in each layer of the ANFIS architecture are briefly explained here, whereas the greater details are available elsewhere in [24, 25].

- Layer 1: each node in this layer contains adaptive node functions in which they are used to map or fuzzify the inputs, x and y, into the corresponding fuzzy linguistic values of *SMALL*, *MEDIUM* or *HIGH* using fuzzy MFs. Fuzzification of the output, O_i^1 in this layer is given by:

$$O_i^1 = \mu A_i(x), i = 1, 2. \tag{2}$$

  where $\mu Ai(x)$ denote the MFs of corresponding linguistic value. In general, the MF can take the form of linear function such as a triangular and trapezoidal function or a nonlinear function like a generalised bell-shaped, Gaussian or a sigmoid function.
- Layer 2: in this level, the fixed node function provides the strength of layer 2 output signal rules, O_i^2 by multiplying the input signals from Layer 1. The multiplication of the incoming signals is given by:

$$O_i^2 = \omega_i = \mu A_i(x) \times \mu B_i(x), i = 1, 2. \tag{3}$$

- Layer 3: this layer calculates the normalised strength of the fuzzy rules, $\overline{\omega}_i$, obtained from the previous layer. This is achieved through:

$$\overline{\omega}_i = \omega_i \Big/ \sum_{i=1}^{n} \omega_i, i = 1, 2. \tag{4}$$

- Layer 4: defuzzification of the first-order Takagi–Sugeno-type fuzzy rules to solve the overall weighted output, $\overline{\omega}_i f_i$, , using weighted average, $\overline{\omega}_i$ is performed in this layer. Typically, defuzzification is accomplished using the following expression:

$$\overline{\omega}_i f_i = \overline{\omega}_i (p_i x + q_i y + r_i), i = 1, 2. \tag{5}$$

- Layer 5: finally, the overall output is calculated using the sum of all weighted signals from layer 4. This is given by:

$$f = \overline{\omega_1} f_1 + \overline{\omega_2} f_2 = (\overline{\omega}_1 x)p_1 + (\overline{\omega}_1 y)q_1 + (\overline{\omega}_1)r_1 + (\overline{\omega}_2 x)p_2 + (\overline{\omega}_2 y)q_2 + (\overline{\omega}_2)r_2 \quad (6)$$

where f_1 and f_2 are the Takagi–Sugeno first-order linear functions, p_1, q_1, p_2, q_2 are the linear parameters of those functions.

3.2.3 Learning algorithm of ANFIS model

The ANFIS model applies hybrid learning algorithms of the gradient descent and the least-squares estimation in order to tune the FIS parameters to match the training data. Specifically, during the forward pass of neural network, function signals go forward until Layer 4 so that the consequent parameters can be optimised by the least-square estimates in order to determine the error rates [24, 25]. During the backward pass, error rates are propagated backward to update or fine-tune the premise parameters by the gradient descent [24, 25]. These learning or training processes continue until the desired number of training iterations (epochs) has been reached, or when the lowest root mean square error (RMSE) between the measured and the generated output has been achieved [28].

4 Results and discussion

4.1 Results from experiments

Figure 3 exhibits the tool wear growth under different cutting speeds, s, fibre orientations, A and constant feed rate, f of 0.16 mm/rev. In general, tool wear increases substantially with a higher cutting speed as expected from the Taylor's model, $V_c T^n = C$ [2, 33, 35]. Interestingly, it is evident that a mild flank wear growth was experienced when the tool was fed across the fibre orientation, A=90°, as compared to along the fibre orientation, A=0°. This results in a longer machining period prior to reaching the critical tool wear criteria. It was not initially anticipated; although Hocheng et al. reported similar trends when machining carbon fibre-reinforced composites (CFRP) [34], under relatively milder machining conditions compared to those employed herein. The difference in the growth rate of tool wear can most likely be attributed to the tool/fibre contact mechanism during machining (i–ii in Fig. 1). When the tool is fed along the fibre direction, increasingly intense contact and rubbing actions between the fractured fibres and each cutting flute

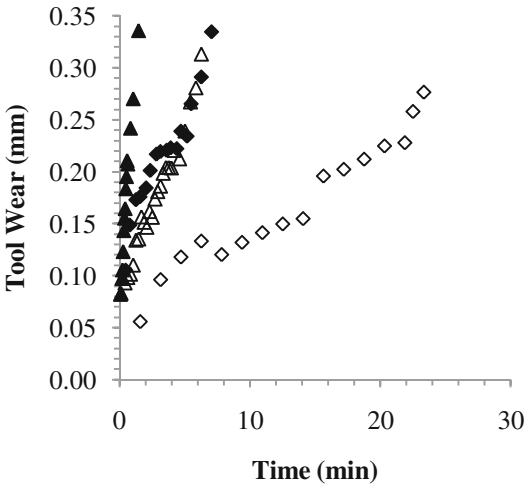

	Cutting speed, s	
Fibre orientation	150 m/min	230 m/min
0°	◆	▲
90°	◇	△

Fig. 3 Tool wear growth at different cutting speed and fibre orientation with constant feed rate of 0.16 mm/rev

can be observed. This is apparent as the undeformed chip thickness changes from small at the entry position of cutting to its maximum at the centre of cutting during a single tool rotation cycle (i in Fig. 1). At the centre position (denoted by the red circle), each of the cutting flutes fractures the fibres orthogonally, which results in the broken fibres rubbing directly on the tool flank face to abrade the tool material. As each of the cutting flutes continues the rotating motion from the centre position, the rubbing actions were maintained at a similar rate. Moreover, since the tool is fully immersed into the workpiece, the cutting mechanisms promote a similar rate of abrasion for each single rotation of the cutting tool.

When the tool was fed across the fibres (ii in Fig. 1), maximum direct contact between the tool and the fibres is only at the entry and exit points of the workpiece. At these positions, the undeformed chip thickness is the smallest, while the contact time between fractured fibres and the tool flank face is relatively short. Although chip loading is the highest at the centre position of cutting (denoted by a red circle shown in ii of Fig. 1), each of the rotating cutting flutes seems to be sliding along the fibres instead of fracturing them. Apparently, the fibres fail due to buckling and bending [34], which alleviate the direct rubbing of the fibres on flank face of the cutting tool. Hence, on the basis of this, a lower rate of tool wear or longer time to arrive at the predefined tool life criteria (Fig. 3) is observed.

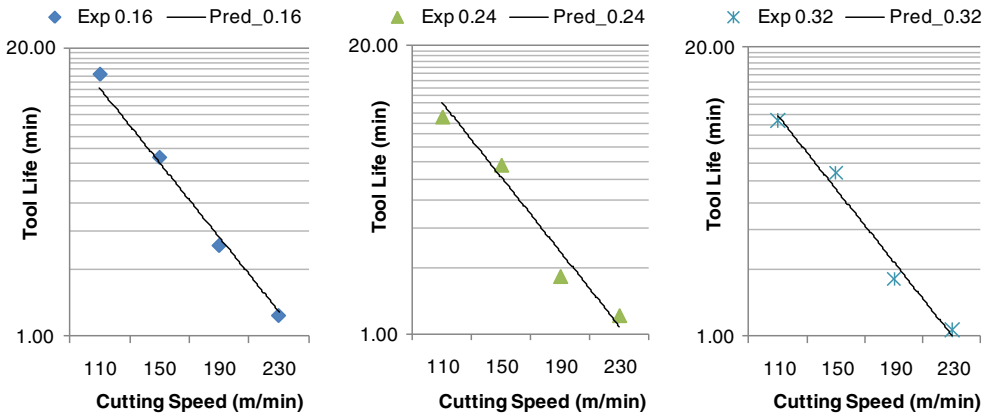

Fig. 4 Variations of predicted and experimental tool life during end milling of GFRP composites

Nevertheless, the tool wear growth for all machining parameters employed in this study follows the typical Taylor's tool wear curve. Hence, the generalised Taylor's tool useful life equation can be derived to predict the tool life during end milling of GFRP composites. Based on the wear criterion of 0.3 mm, the tool life of each machining parameter can be estimated from the tool wear curves. Using these values, the Taylor's tool useful life equation, TL, derived as a function of cutting speed, s and feed rate, f is given by:

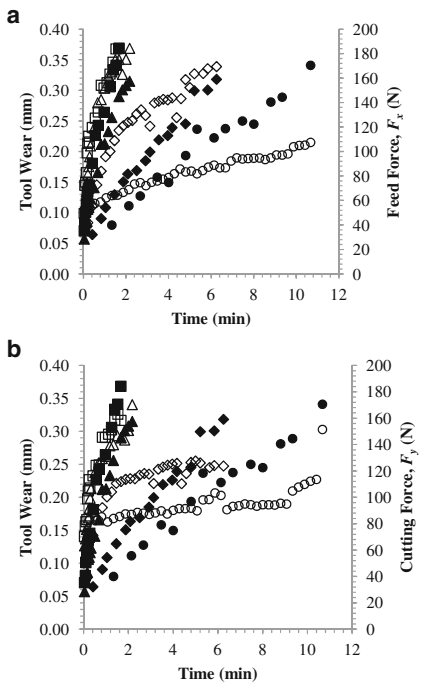

Cutting Speed	110 m/min	150 m/min	190 m/min	230 m/min
Tool Wear	●	◆	▲	■
Force	○	◇	△	□

Fig. 5 Tool wear growth and machining force development at different cutting speed and constant feed rate of 0.24 mm/rev for: **a** feed force, F_x and **b** cutting force, F_y

$$TL = 10^{7.279} \times s^{-3.161} \times f^{-0.422}, R^2 = 0.969 \quad (7)$$

When fibre orientation, A, is taken into account, a more general Taylor's equation is given in Eq. 8:

$$TL = 10^{0.351} \times s^{-0.722} \times f^{-0.251} \times A^{0.445}, R^2 = 0.946 \quad (8)$$

Judging from the R^2 values of 0.969 and 0.946, it can be concluded that both equations can describe the experimental trend very well. In addition, the results from these statistical analyses suggest that cutting speed has the dominant influence on the TL. This was based on the exponents of the derived Taylor's equation, Eq. 7, in which $n_1 > n_2$ and $n_1 > n_3$ (where n_1, n_2 *and* n_3 are the exponents for cutting speed, feed rate and fibre orientation, respectively). Moreover, the expected inverse relationship of cutting speed with tool useful life is in agreement with recently reported study on drilling of CFRP composites [36]. Hence, this warrants it to conclude that the tool life/wear is essentially or highly dependent on the cutting speed. Although the change of orientation certainly affects the rate of tool wear, surprisingly, the resulting exponent of Eq. 8 indicates that the influence of fibre orientation on TL is marginal compared to that of the machining parameters. This is despite the two fibre orientations studied herein are the extremes as far as the tool wear growth is concerned.

From the aforementioned discussion, it may be said that the wear and critical life of the cutting tool during end milling of this composite material are mainly governed by mechanical actions of the tool rotation and table feed during machining. Indeed, the combinations of these parameters contribute to the aggressive rubbing of the fibre reinforcements on flank face of the cutting tool. This results in a rapid increase of heat energy being absorbed by the tool during machining to accelerate the wear, and consequently reduces the tool life. In contrast, the fibre orientation plays an opposite role in influencing the tool wear growth and determining the critical tool life. As apparent, the effect of

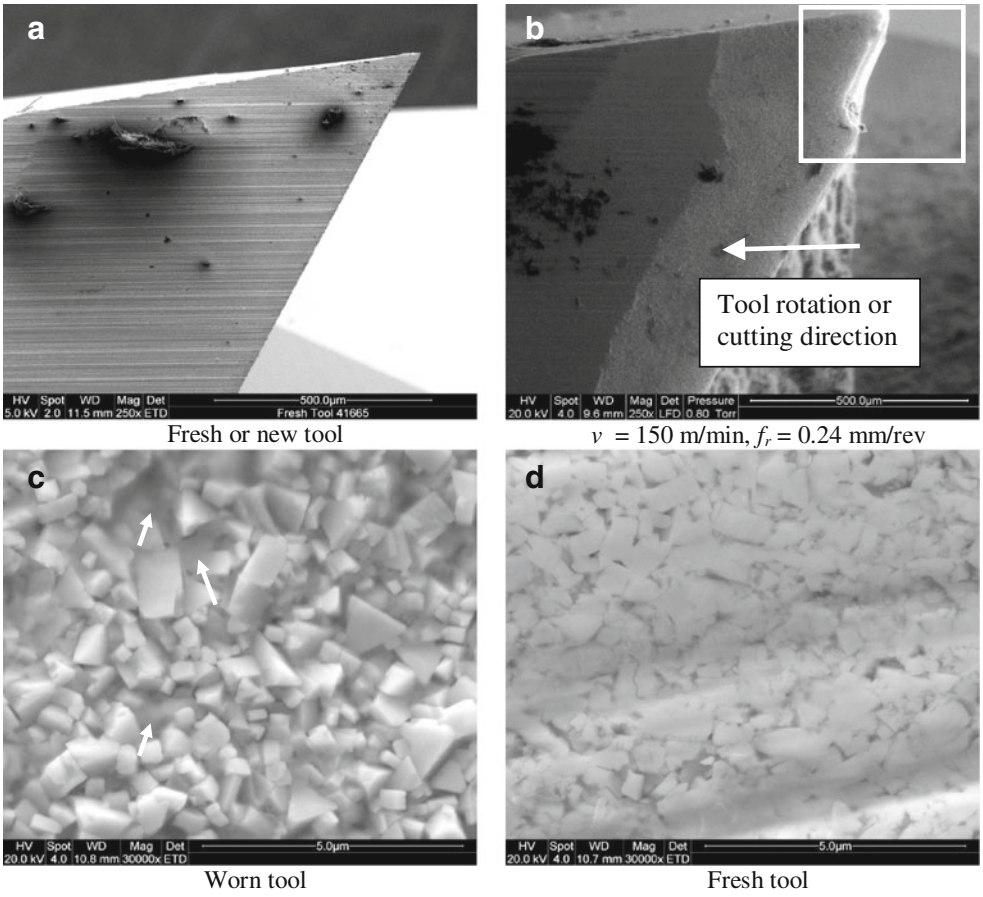

Fig. 6 Tool wear mechanisms during end milling of GFRP composites

changing fibre orientation of the GFRP composites is not large enough to offset the results of increasing machining parameters. Furthermore, due to the fact that milling is a highly complex machining process that involves oblique cutting mechanisms, fibre orientation, A, cannot be easily controlled as minute changes of fibre/tool contact which takes place continuously during the engagement of the tool with the workpiece material.

The variations of predicted TL with the measured experimental data are displayed in Fig. 4 for different cutting speeds and feed rates. The mean absolute percentage error (MAPE) has been found to be within 15 %. More encouraging results are exhibited when additional tests under randomly chosen parameters of s=170 m/min, f=0.24 mm/rev with A=0° and s= 190 m/min, f=0.32 with A=45°, are performed. Experimental tool life, $TL_{exp\_A=0}$ has been recorded to be 3.00 min, whereas, the calculated or predicted tool life, $TL_{predicted\_A=0}$ is 3.09 min. As for A=45°, slightly higher prediction of tool life is observed, $TL_{predicted\_A=45}$ is 3.24 min in comparison to 3.38 min obtained from the experiment. The resulting percentage errors between the predicted and experimental data of TL are 3.00 % and 4.29 % respectively. Hence, the derived equations can be used with a reasonably accuracy to predict the useful life of the end mill tool when machining GFRP composites.

Apart from the tool wear growth, variations of machining forces were regularly monitored for each end milling pass until the end of tool life. Figure 5 demonstrates the trends of feed force (F_x) and cutting force (F_y) magnitudes, with respect to machining time for the given machining parameters. The feed and cutting forces can be seen to consistently increase up to maximum values of 230 and 209 N, respectively. Since the variations of machining forces follow similar trends as that of the tool wear growth, it can be asserted that these variations are due to the growth of the tool wear. Hence, the measured machining force can be directly used to indicate the extent of tool wear. A later section will discuss the development of tool wear-machining force relationships using statistical analyses and fuzzy logic modelling.

Scanning micrographs of the worn tool (Fig. 6), have confirmed that the tool wear or failure mechanism observed in this set of experiments is predominantly due to abrasion on the flank face of each cutting flute. It is apparent that two-body abrasion between the fibres and the tool flank face, results in the uniform scratch marks along the tool rotation or cutting direction. The marks caused by rubbing actions of the fibres are noticeable on flank face of the worn tool which can be verified by comparing with the condition of the new or fresh tool (Fig. 6a). On the other hand, the

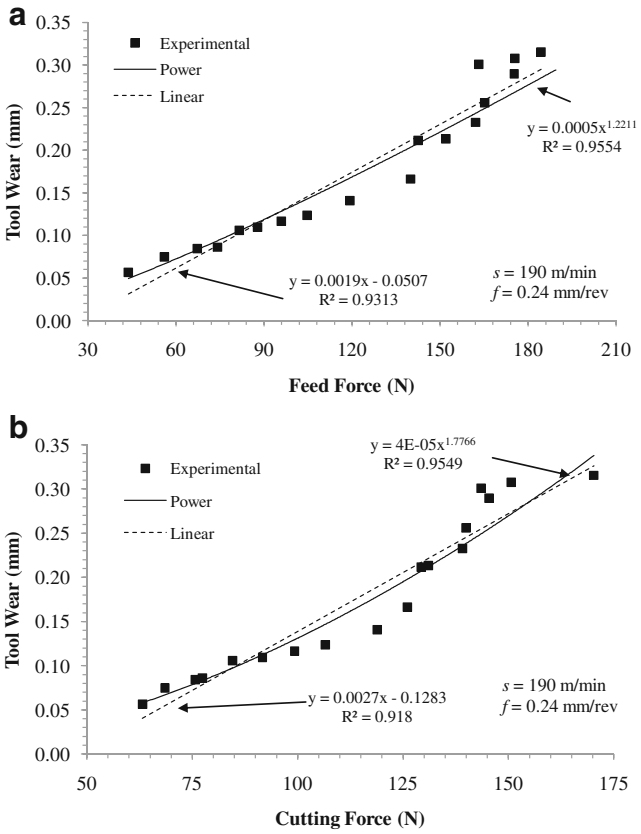

Fig. 7 Individual regression results for **a** feed force, F_x, and **b** cutting force, F_y

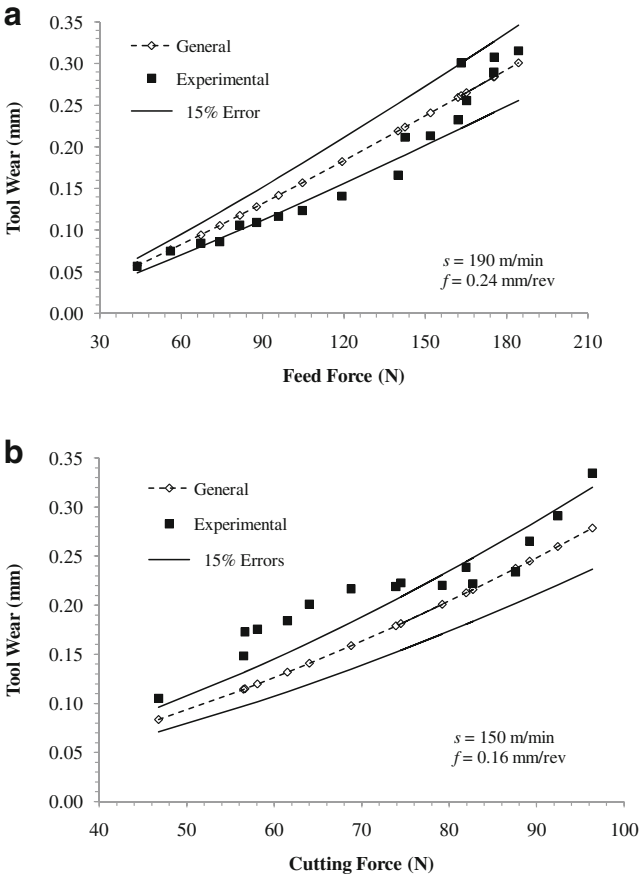

Fig. 8 Comparison of experimental and predicted data from MRA for **a** feed force, F_x, and **b** cutting force, F_y, under different machining conditions

intermittent end milling cutting process and high fluctuation of machining forces when machining this composite material promote some micro-chipping on the edges of the cutting tool, as indicated by the white coloured box in Fig. 6b. A comparison of a higher magnification microstructure of the new/fresh tool surface and the worn tool surface is shown side by side in Fig. 6c–d. It is evident that the tungsten carbide (WC) grains appeared to be closely bonded together with the cobalt binder (Fig. 8c) prior to the machining process. As the tool wears out, voids on the tool surface are clearly visible as pointed-out by the arrows (Fig. 6d). These microstructure characteristics indicate that the cobalt binders between the WC grains are severely removed by the highly abrasive fibre reinforcements. As the machining process continues, the fractured fibres can penetrate between the WC grains under high machining pressure to further erode the cobalt binder and fracture the larger WC grains into smaller fragments. The wear phenomenon discussed herein was also observed by Sheikh-Ahmad et al. when turning fibreboards [32].

4.2 Results of statistical modelling using MRA

During the first stage of statistical analysis, basic regression fittings were performed on individual machining parameters employed in this study in order to understand relationships between tool wear and the machining forces. Experimental data were fitted using both linear and power law functions for feed force, F_x and cutting force, F_y (Fig 7a and b), respectively. From these individual analyses, it appears that the changes of tool wear with magnitude of machining forces can be fairly modelled using both functions. However, the power law function yields a more accurate result to match the experimental data, judging from the R^2 values for most machining parameters. Therefore, following the power

Table 2 Details of ANFIS training and checking datasets

Input/ Output variables	Training data range		Validation data range	
	Minimum	Minimum	Minimum	Minimum
Cutting speed, s (m/min)	110	230	150	230
Feed rate, f (mm/rev)	0.16	0.32	0.16	0.24
Feed force, F_x (N)	25	230	50	173
Cutting Force, F_y (N)	41	210	70	158

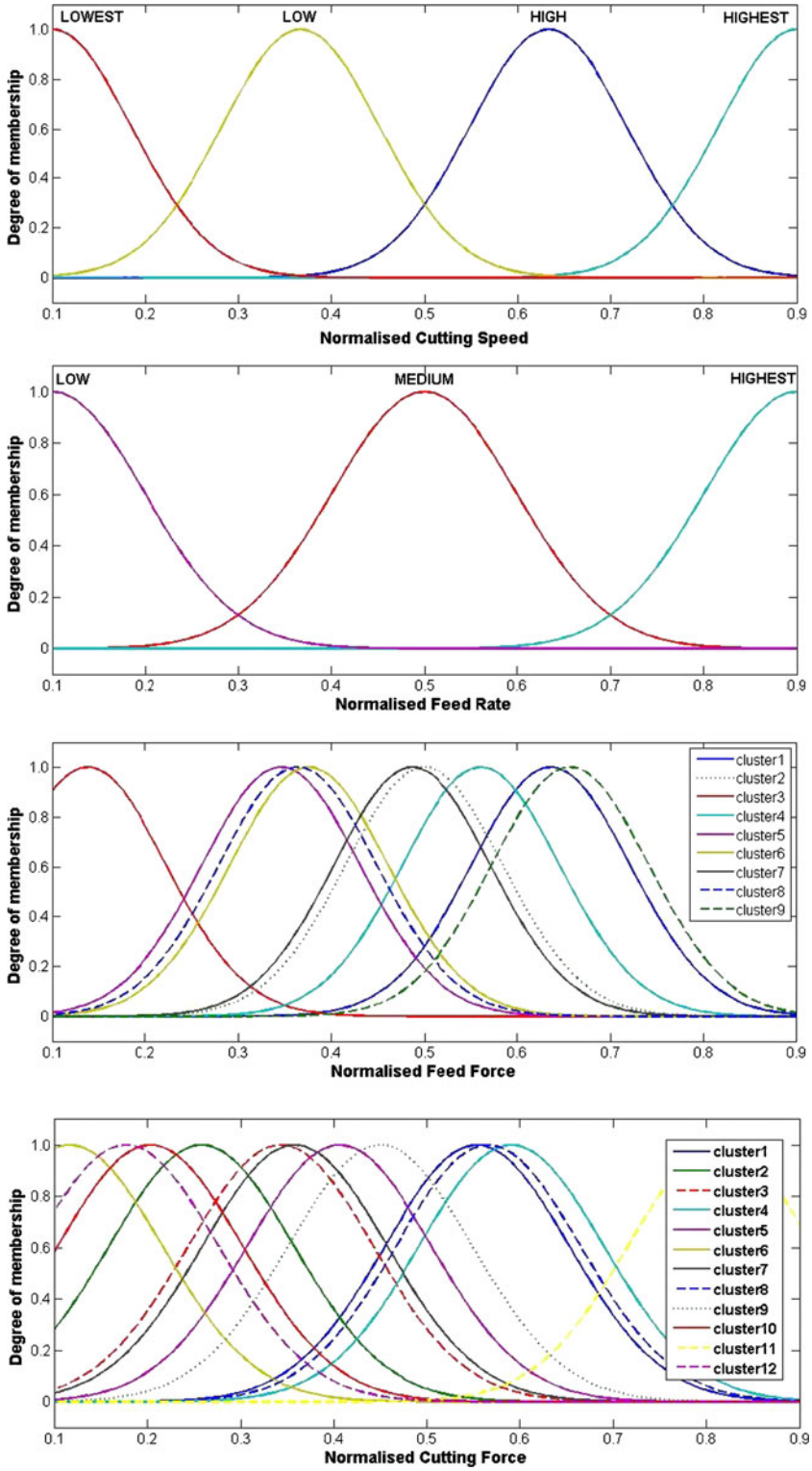

Fig. 9 Initial Gaussian MFs for all input prior to ANFIS training

law function, general tool wear-machining force relationships representing different machining parameters employed in this work were then derived using MRA. As previously discussed, fibre orientation was not deemed to be critical due to its relatively low influence on tool life based on the derived Taylor's model, Eq. 8. As far as machining is concerned, cutting speed and feed rate are still the governing parameters to influence the tool life or tool wear. Hence, fibre orientation has not been used as one of the input variables to derive the empirical models. Considering feed

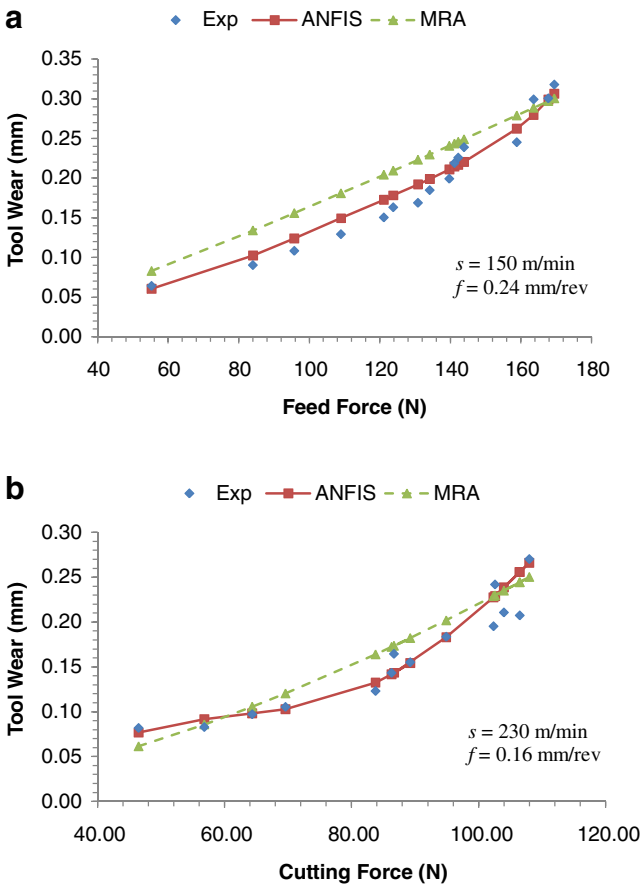

Fig. 10 Comparison of experimental, MRA- and ANFIS-predicted data for **a** feed force, F_x, and **b** cutting force, F_y, under different machining conditions

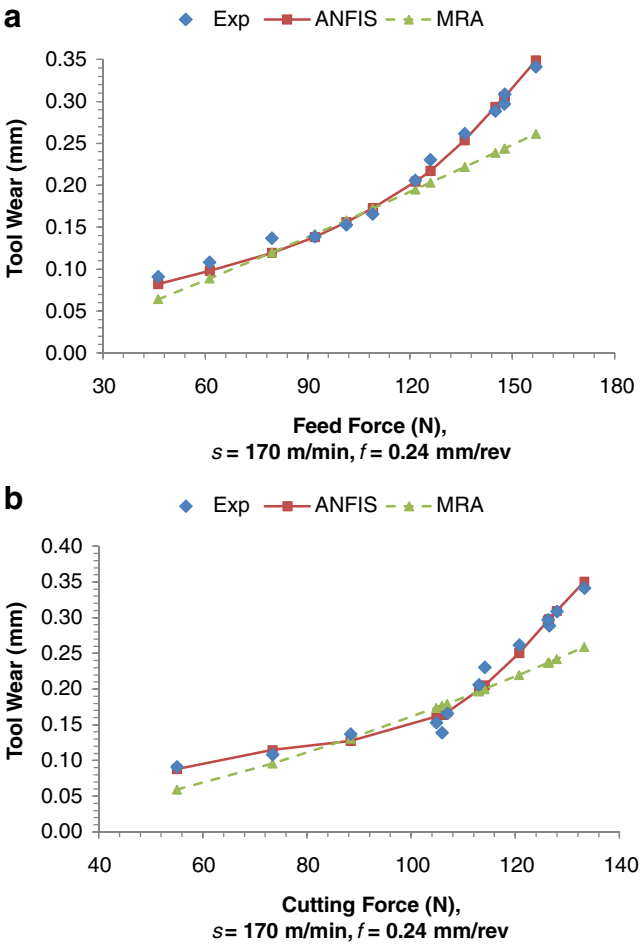

Fig. 11 Comparison of experimental, MRA- and ANFIS-predicted data for **a** feed, F_x, and **b** cutting force, F_y, for the checking datasets

and cutting forces separately, the derived general equations from MRA are given by Eqs. 9 and 10, respectively:

$$TW = 10^{-2.547} \times s^{-0.409} \times f^{-0.564} \times F_x^{1.150}, \quad R^2 = 0.851 \tag{9}$$

$$TW = 10^{-3.382} \times s^{-0.694} \times f^{-1.296} \times F_y^{1.667}, \quad R^2 = 0.821 \tag{10}$$

where TW is tool wear (in millimeter), s is the cutting speed (in meters per minute), f is the feed rate (in millimeters per revolution), and F_x (in newton) and F_y (in newton) are feed and cutting forces, respectively. Overall, based on the R^2 values, the results of these multiple regression analyses suggest that the derived general equations can predict the trend of tool wear with acceptable accuracy. However, it is evident that the tool wear-feed force equation gives a slightly better prediction on the extent of tool wear as compared to the tool wear-cutting force relationship. The calculated results using Eqs. 9 and 10 are displayed in Fig. 8 for two selected machining parameters employed in this work. The predicted TW from the tool wear-feed force relationship, Eq. 9, appears to be satisfactory, as most of the experimental data lie within the ±15 % error zone (compared to the predicted values) (Fig. 8a). However, the tool wear-cutting force relationship seems to underestimate the extent of tool wear (Fig. 8b), within certain cutting force region. Scattering of the experimental data from the predicted or calculated TW is evident with only part of them being within ±15 % zone. Owing to the nature of intermittent or discontinuous cutting actions during end milling and random variations in the material properties, inherent scattering or fluctuation of the measured cutting force data is observed. This is obvious as the tool fractures the non-homogeneous layers of fibre reinforcements and epoxy matrix with different chip sizes. On the basis of these factors, slightly poorer results are obtained in the regression analysis, Eq. 10.

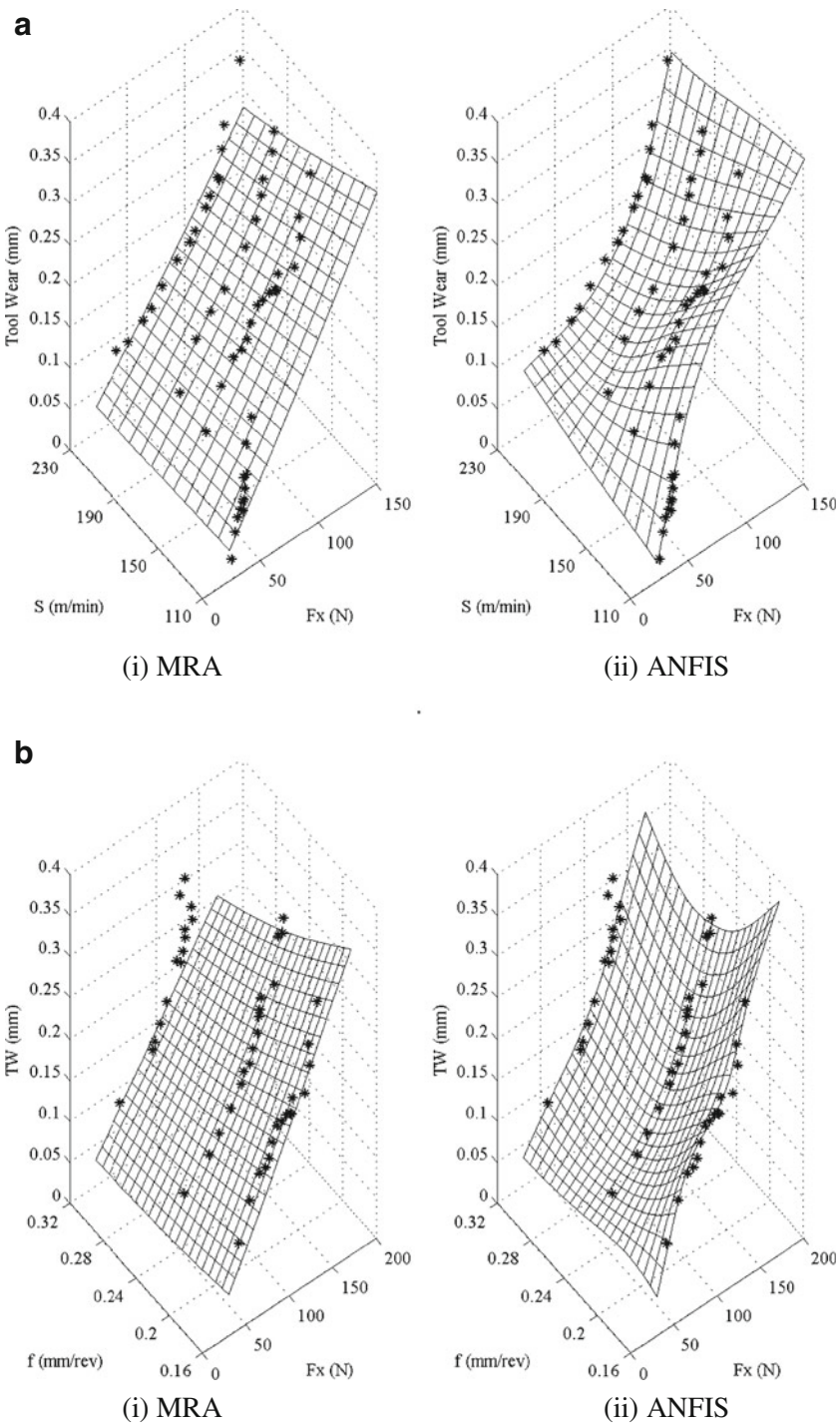

Fig. 12 **a** 3D surface diagram of (*i*) MRA- and (*ii*) ANFIS-predicted data superimposed upon the experimental data for feed force, F_x ,at f=0.16 mm/rev, **b** 3D Surface diagram of (*i*) MRA- and (*ii*) ANFIS-predicted data superimposed upon the experimental data for feed force F_x, at s=150 m/min

4.3 Construction of ANFIS model and its results

Due to the anisotropic and inhomogeneous properties of GFRP composites, variations in the machining force measurement exist. Hence, highly accurate constitutive relationships of tool wear-machining forces are difficult to be established by the method of regression analysis, as shown earlier. Therefore, in this section, the application of advanced fuzzy logic modelling, known as ANFIS is demonstrated for improving of the tool wear prediction. Prior to the ANFIS modelling, restructuring of the datasets was performed to enhance the predictive capability of the ANFIS model. Firstly, feed and cutting force datasets were normalised between 0.1 and 0.9 in

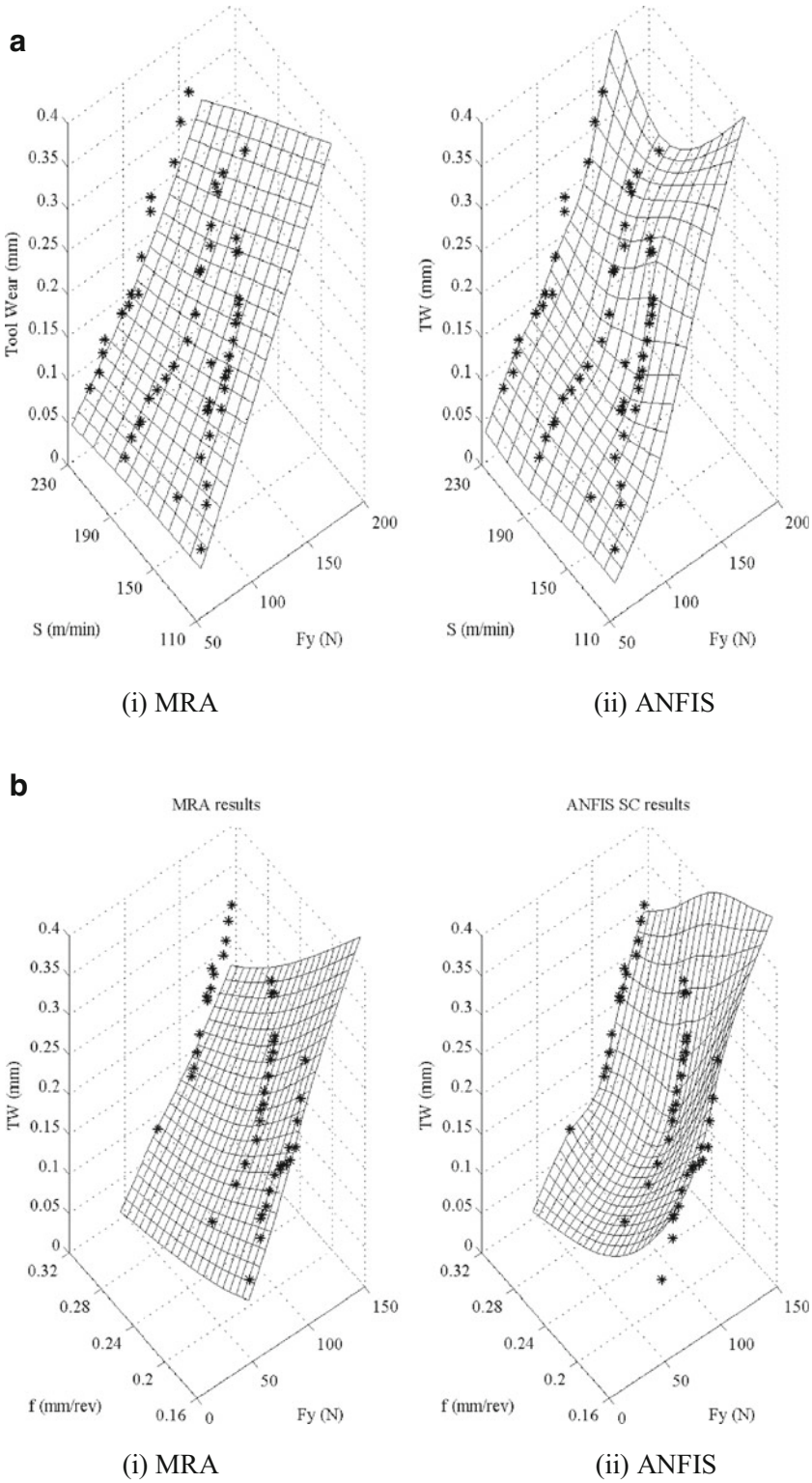

Fig. 13 **a** 3D surface diagram of (*i*) MRA- and (*ii*) ANFIS-predicted data superimposed upon the experimental data for cutting force, F_y ,at f=0.24 mm/rev, **b** 3D Surface diagram of (*i*) MRA- and (*ii*) ANFIS-predicted data superimposed upon the experimental data for cutting force, F_y, at s=150 m/min

order to produce uniform non-dimensional experimental data. This was carried out using the following expression:

$$x_n = 0.1 + 0.8 \times \left(\frac{d_i - d_{\min}}{d_{\max} - d_{\min}} \right) \tag{11}$$

where $d_{\max}$ and $d_{\min}$ are the maximum and minimum values of raw data while d_i is the ith data point of a dataset. For better generalisation of an ANFIS model, the normalised data are randomised and divided into training and validation datasets as would normally be performed in any neural network model. Machinability data and/or experimental results gathered from

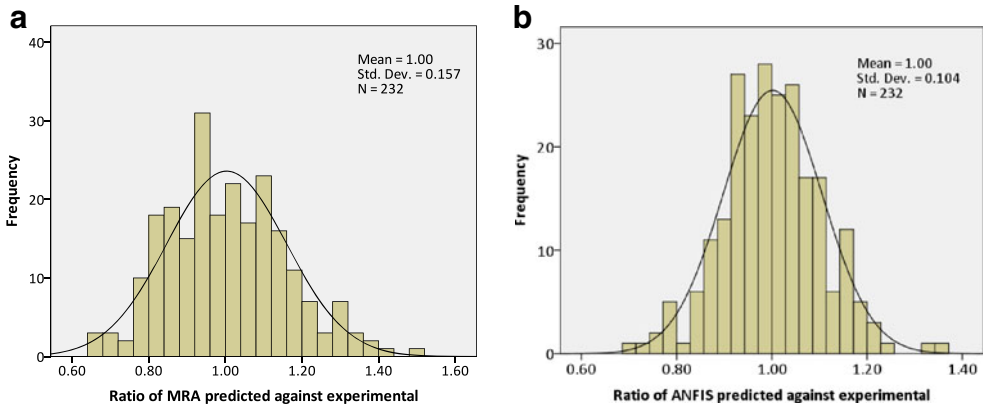

Fig. 14 Histogram of ratio between predicted value against experimental data for **a** MRA_F_x and **b** ANFIS_F_x

the wide range of experiments (Table 1) were used for training of the ANFIS model. The validation of the trained ANFIS model was then implemented using new input data from repeated experiments of randomly selected machining parameters. Obviously, the new datasets were different from the training datasets. Table 2 summarises the range of values for training and validation input–output datasets used to develop the ANFIS predictive models. Similar to that of MRA, two different ANFIS models were constructed using feed and cutting force datasets to predict a single output variable, tool wear, TW. This approach offers the flexibility of having different types of MFs in the ANFIS architecture. An important element in the ANFIS modelling is the selection of parameters for fuzzy inferencing, which are the type and number of MFs. These parameters are essential to form the antecedent or premise parameters of the fuzzy rules. In the current work, the developed ANFIS model employed the nonlinear Gaussian MFs for each of the input data (cutting speed, feed rate and machining forces). The smoothness and symmetrical shape of the Gaussian function curves make them suitable for the development of these highly nonlinear tool wear-machining force relationships. Typically, a Gaussian membership function, which spreads across the experimental input range with maximum and minimum degree of membership range from 0 to 1, is given by:

$$\mu A_j^i = \exp\left[\frac{-\left(x_j - a_j^i\right)^2}{2b_j^2}\right] \tag{12}$$

where x is the input parameter, and a and b are the Gaussian function parameters which will be optimised in the subsequent input space partitioning stage. Parameter a represents the Gaussian function centre (mean) whereas b determines the width (standard deviation) of the Gaussian function. The aforementioned input space partitioning of the training datasets was performed using subtractive-clustering technique in order to determine the optimum number and size of the Gaussian MFs and fuzzy rules required for the ANFIS model. Both parameters were determined based on the number of cluster centres obtained from the clustering technique. This technique assumes that each data point can be a potential cluster centre and calculates the likelihood of each selected point being the cluster centre [24–26]. The potentiality of being a cluster centre is based on the density of surrounding data points. Results of applying the subtractive-clustering

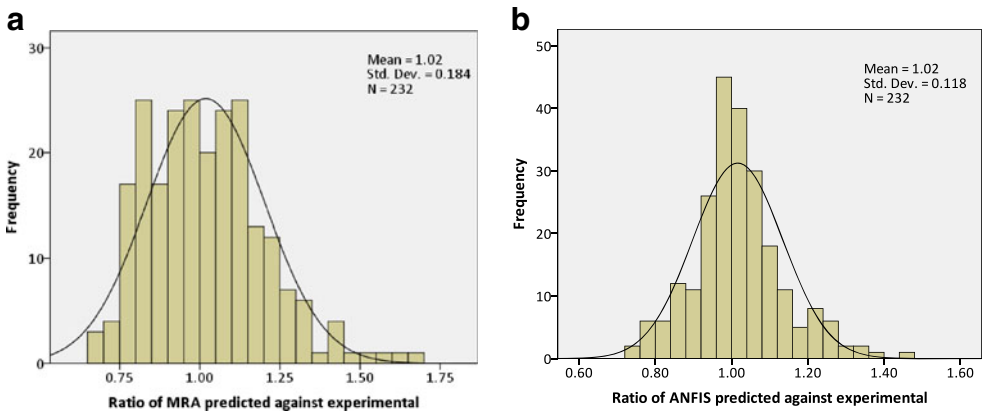

Fig. 15 Histogram of ratio between predicted value against experimental data for **a** MRA_F_y and **b** ANFIS_F_y

Table 3 Statistical comparison of the MRA and ANFIS predictive performance

	Tool wear-F_x MRA modelling	Tool wear-F_x ANFIS modelling	
	All datasets	Training datasets	Validation datasets
R^2	0.9789	0.9920	0.9933
RMSE	0.0294	0.018	0.016
cov (%)	15.52	9.56	8.87
MAPE	12.64	8.20	6.74
	Tool wear-F_y MRA modelling	Tool wear-F_y ANFIS modelling	
	All datasets	Training datasets	Validation datasets
r^2	0.9744	0.9889	0.9877
RMSE	0.033	0.021	0.022
cov (%)	17.50	11.29	12.06
MAPE	15.14	8.66	8.67

technique to the current datasets produced 9 to 12 Gaussian MFs, which were spaced over the range of input parameters (Fig. 9). It is imperative to note that the purpose of using clustering method is to identify natural groupings of data so as to produce a concise representation of large dataset. Following the clustering of input data, the neural network training of the ANFIS model was performed in several epochs (iterations) using the predetermined number of Gaussian MFs and fuzzy rules in order to identify the final ANFIS models for tool wear prediction. The fuzzy rules formulated in the model are shown here for one of the ANFIS models developed:

R1 If (Cutting Speed is HIGH*) and (Feed Rate is* MEDIUM*) and (Feed Force is* CLUSTER1*) then (*TW*1*$= p_1 s + q_1 f + r_1 F_x + s_1$*)*

R9 If (Cutting Speed is HIGH*) and (Feed Rate is* MEDIUM*) and (Feed Force is* CLUSTER9*) then (*TW$= p_9 s + q_9 f + r_9 F_x + s_9$*)*

These formulated rules were implemented using Takagi–Sugeno-type FIS in the MATLAB Fuzzy Logic Toolbox environment. Repeated training and checking of the ANFIS neural network module were performed until the minimum training error has been achieved. A comparison of ANFIS-predicted outputs with the MRA-calculated results and experimental data are displayed for feed and cutting forces (Fig. 10a and b), respectively. In both cases of ANFIS and MRA modelling, it can be seen that the tool wear-force relationship follows a linear trend in the lower machining force region (at approximately less than 80 N). However, as the high machining force region approaches, ANFIS models show a remarkable match to the experimental data. This may indicate that the functional relationship has changed to nonlinearity. Indeed, with the hybrid learning algorithms of gradient descent and backpropagation network of ANFIS architecture, as well as the application of nonlinear Gaussian functions as the fuzzy logic MFs, a highly accurate prediction of the tool wear is displayed throughout the entire force range. On the contrary, it is noticeable that change in the functional relationships, particularly in the high machining force range, could not be closely fitted by MRA technique (Fig. 10). This is likely to be a result of linear interpolative nature of the MRA which results in a continuous linear relationship between tool wear and the machining force. Similar trends exist for validation datasets, which were implemented on the final ANFIS trained models. Notably, an excellent fit of predicted values against experimental data is also evident for the selected validation datasets (Fig. 11).

Since a wide range of machining parameters was employed, it was possible to plot 3D surface diagrams of predicted values obtained from each modelling technique superimposed with the experimental data. These plots (Figs. 12 and 13) provide a clearer representation of how well the predicted values fit the experimental data. From these plots, it is evident that the MRA-predicted values show a linear trend within all force levels. In contrast, it appears that the accuracies of the ANFIS models are well pronounced throughout all machining force levels, as shown in both figures. As indicated earlier, the apparent difference between them can be easily noticed in the high machining force region.

4.4 Statistical and error analyses of the MRA and ANFIS models

The ratios of predicted values to experimental data for each of the developed models are presented using histograms in order to compare their statistical characteristics, based on frequency distribution functions (Figs 14 and 15). As shown in these histograms, the standard deviations of the calculated ratios are 0.157 and 0.104 for MRA and ANFIS models, respectively for the feed force, F_x, datasets, whereas they are, 0.184 and 0.118 for the cutting force, F_y, datasets. This shows the tendency for the variance of the ratio to decrease with the shift from MRA models to ANFIS models and also from using cutting force data to feed force data in order to predict the tool wear. Hence, this supports the results of regression analysis presented earlier with regard to better accuracy of tool wear-feed force relationship. In addition, the performance of the developed tool wear prediction

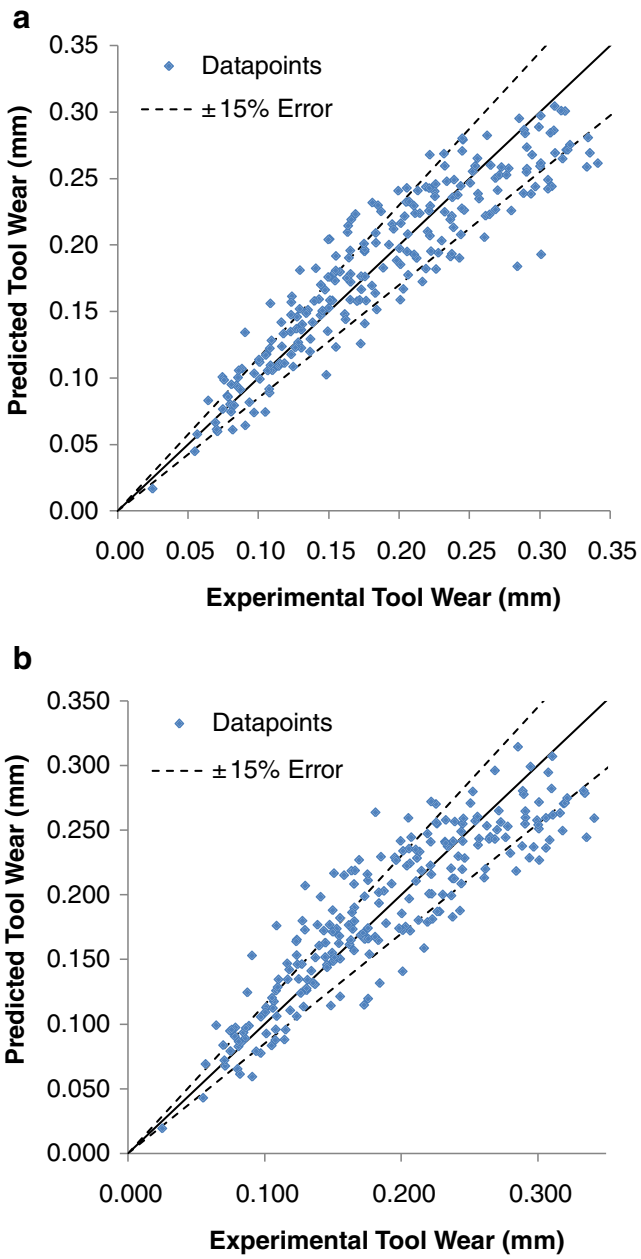

Fig. 16 **a** Scatter diagram of MRA-predicted values against experimental data for F_x, **b** scatter diagram of MRA-predicted values against experimental data for F_y

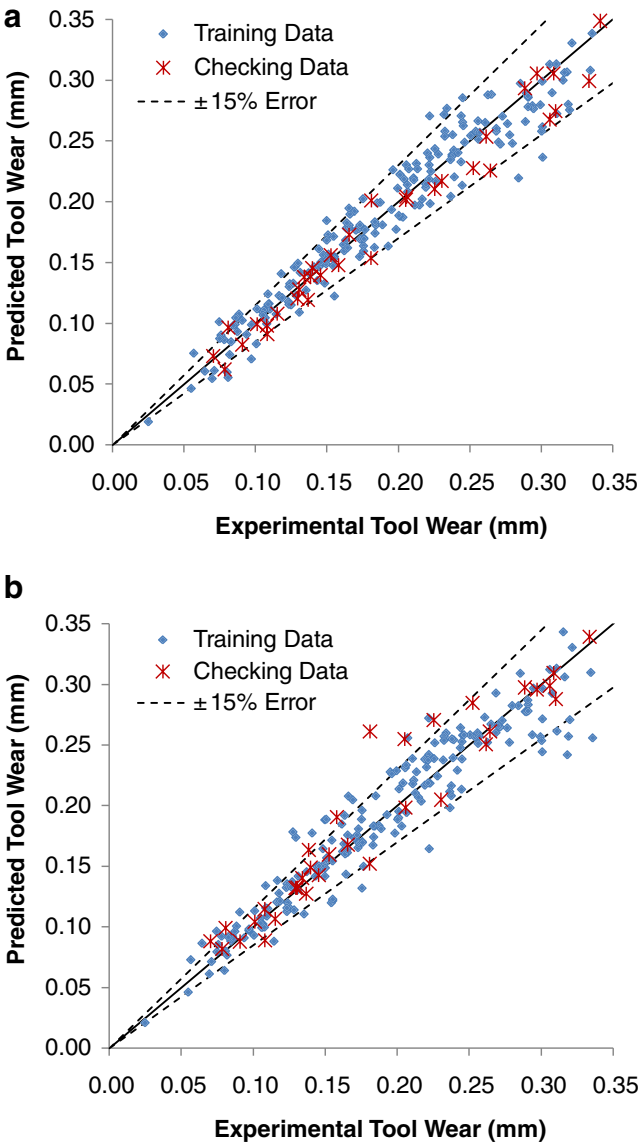

Fig. 17 **a** Scatter diagram of ANFIS-predicted values against experimental data for F_x, **b** scatter diagram of ANFIS-predicted values against experimental data for F_y

models was evaluated using several statistical indices. The indices are in terms of statistical error measures namely, the RMSE, the coefficient of variation (cov.), the absolute fraction of variance (R^2) and the MAPE. The equations for these statistical error measures are as follows:

$$RMSE = \sqrt{\frac{\sum_{i=1}^{m}\left(y_{pred,i} - y_{\exp,i}\right)^2}{m}} \tag{14}$$

$$cov. = \frac{RMSE}{\left|\overline{y}_{\exp}\right|} \tag{15}$$

$$r^2 = 1 - \frac{\sum_{i=1}^{m}\left(y_{pred,i} - y_{\exp,i}\right)^2}{\sum_{i=1}^{m}\left(y_{\exp,i}\right)^2} \tag{16}$$

$$MAPE = \frac{\sum_{i}^{m}\left(\frac{y_{pred,i} - y_{\exp,i}}{y_{pred,i}}\right) \times 100}{m} \tag{17}$$

where, $y_{\text{pred},i}$ and $y_{,\text{exp},i}$ are the predicted value and experimental data of the tool wear respectively, $\bar{y}_{\text{exp}}$ is the average experimental data of tool wear and m is the number of sample. Table 3 compares the results of statistical performances for each of the developed predictive models. It is apparent that the accuracy and improvement of ANFIS predictive capabilities compared to the MRA models. Nevertheless, as mentioned earlier, large variations, fluctuations or noises in the measured cutting force, F_y, render a less accurate prediction of tool wear for both MRA and ANFIS models. Scatter diagrams (Fig. 16) were also plotted to demonstrate the accuracy of the predicted tool wear from MRA models in comparison to the experimental data under all experimental conditions. A perfect prediction would show that all points lie on the 45° line. A ±15 % error zone line is imposed along the 45° line to display how close the comparative data points are bunched together. Comparatively, there are a number of data points, scattered outside the error zone for both the MRA models indicating only acceptable accuracy in the MRA predictive capabilities. Likewise, scatter diagrams displaying all predicted values of tool wear from the ANFIS models against the measured tool wear were also plotted (Fig. 17). It can be seen that almost all predicted data clustered within ±15 % error and close to the 45° line (for perfect prediction). Hence, this indicates the significant improvements in the tool wear prediction using ANFIS models for both feed and cutting force datasets.

5 Concluding remarks

This paper has presented the results of end milling machinability tests of GFRP composites using uncoated tungsten carbide tools. The Taylor's tool life equations have been derived to determine the useful life of the end mill cutter. Additionally, tool wear-machining force models have been developed in order to monitor the extent of tool wear during end milling of these composite materials. The following conclusions can be drawn from the results presented earlier:

- An increased cutting speed or feed rate accelerates the tool wear growth and leads to rapid failure of the cutting tool.
- Machining across the fibre orientation (90° to fibre orientation) eases the growth of the tool wear which eventually prolongs the tool useful life when compared to machining along the fibre orientation (0°). The marginal increase of tool wear when machining at 90° fibre orientation is likely due to inherently tool/fibre contact.
- The derived Taylor's equations have confirmed that the useful life of the end mill cutter is strongly influenced by cutting speed and feed rate.
- As indicated in the equations, the effect of machining at the two fibre orientations does not show significant influences on the tool life as compared to those for varying machining parameters.
- The progression of tool wear can be effectively monitored without interrupting the cutting process by using the derived relationships between tool wear and machining forces. General equations from MRA (based on power law function) exhibit an acceptable accuracy in predicting the extent of tool wear when compared to the experimental data.
- The evidence is highly conclusive that reasonably accurate tool wear prediction can be easily achieved using the feed force, F_x, data rather than the cutting force, F_y.
- The ANFIS models applied on the same dataset has yield a significant improvement in predicting the tool wear during end milling of the composite materials. Results show that the developed ANFIS models exhibit highly accurate predictive capabilities, especially when the functional relationships are nonlinear. The ANFIS superiority is attributed to the hybrid learning algorithms of backpropagation and gradient descent, as well as the application of the nonlinear Gaussian function as the fuzzy logic membership function.

Acknowledgments Funding provided by Ministry of Higher Education Malaysia (MOHE) and Universiti Malaysia Perlis (UniMAP) during the PhD course of the first author is immensely appreciated. The financial support from the University of Auckland Press (UoA Press) account is acknowledged. The authors also thank the technical staff at the Centre for Advanced Composite Materials, The University of Auckland for the experimental help rendered.

References

1. Santhanakrishnan G, Krishnamurthy R, Malhotra SK (1988) Machinability characteristics of fibre reinforced plastics composites. J Mech Work Technol 17:195–204
2. Klocke F, Koenig W, Rummenhoeller S, Wuertz C (1999) Milling of advanced composites: machining of ceramic and composites. Marcel Dekker, New York
3. Koplev A, Lystrup A, Vorm T (1983) The cutting process, chips, and cutting forces in machining CFRP. Compos 14(4):371–376
4. Sakuma K, Seto M (1981) Tool wear in cutting glass-fiber-reinforced-plastics (the relation between cutting temperature and tool wear). Bull JSME 24:748–755
5. Nayak D, Bhatnagar N, Mahajan P (2005) Machining studies of uni-directional glass fiber reinforced plastic (UD-GFRP) composites part 1: effect of geometrical and process parameters. Mach Sci Technol 9:481–501
6. Rao GVG, Mahajan P, Bhatnagar N (2007) Machining of UD-GFRP composites chip formation mechanism. Compos Sci Technol 67:2271–2281
7. Ramulu M, Wern CW, Garbini JL (1993) Effect of fibre direction on surface roughness measurements of machined graphite/epoxy composite. Compos Manuf 4(1):39–51

8. Iliescu D, Gehin D, Gutierrez ME, Girot F (2010) Modelling and tool wear in drilling of CFRP. Int J Mach Tools Manuf 50 (2):204–213
9. Davim JP, Reis P, Lapa V, António CC (2003) Machinability study on polyetheretherketone (PEEK) unreinforced and reinforced (GF30) for applications in structural components. Compos Struct 62(1):67–73
10. Bhattacharrya D, Allen MN, Mander SJ (1993) Cryogenic machining of Kevlar composites. Mater Manuf Proc 8(6):631–651
11. Bhattacharyya D, Horrigan DPW (1998) A study of hole drilling in Kevlar composites. Compos Sci Technol 58(2):267–683
12. Palanikumar K, Karunamoorthy L, Manoharan N (2006) Mathematical model to predict the surface roughness on the machining of glass fibre reinforced polymer composites. J Reinf Plast Compos 25(4):407–418
13. Kim KS, Lee DG, Kwak YK, Namgung S (1992) Machinability of carbon fiber-epoxy composite materials in turning. J Mater Process Technol 32:553–570
14. Azmi AI, Lin RJT, Bhattacharyya D. (2012) Machinability study of glass fibre reinforced composite during end milling. Int J Adv Manuf Technol In Press: doi:10.1007/s00170-012-4006-6
15. Davim JP, Reis P, Antonio CC (2004) A study on milling of glass fiber reinforced plastics manufactured by hand-lay up using statistical analysis (ANOVA). Compos Struct 64(3–4):493–500
16. Davim JP, Reis P (2005) Damage and dimensional precision on milling carbon fiber-reinforced plastics using design experiments. J Mater Process Technol 160(2):160–167
17. Razfar MR, Zadeh MRZ (2009) Optimum damage and surface roughness prediction in end milling glass fibre-reinforced plastics using neural network and genetic algorithm. Proc Inst Mech Eng Part B 223(6):653–664
18. Chen XQ, Li HZ (2009) Development of a tool wear observer model for online tool condition monitoring and control in machining nickel-based alloys. Int J Adv Manuf Technol 45:786–800
19. Lin JT, Bhattacharyya D, Kecman V (2003) Multiple regression and neural networks analyses in composites machining. Compos Sci Technol 63:539–548
20. Saglam H, Unuvar A (2003) Tool condition monitoring in milling based on cutting forces by a neural network. Int J Prod Res 41 (7):1519–1532
21. Gill SS, Singh R, Singh J, Singh H (2012). Adaptive neuro-fuzzy inference system modeling of cryogenically treated AISI M2 HSS turning tool for estimation of flank wear. Expert Sys Appl 39 (4):4171–4180
22. Lin SC, Lin RJ (1996) Tool wear monitoring in face milling using force signals. Wear 198:136–142
23. Özel T, Karpat Y (2005) Predictive modeling of surface roughness and tool wear in hard turning using regression and neural networks. Int J Mach Tools Manuf 45:467–479
24. Jang JSR (1993) ANFIS: adaptive-network-based fuzzy inference system. IEEE Trans on Sys Man Cybern 23(3):665–685
25. Jang JSR, Sun CT, Mizutani E (1996) Neuro-fuzzy and soft computing: a computational approach to learning and machine intelligence. Prentice-Hall, New Jersey
26. Chiu S (1994) Fuzzy model identification based on cluster estimation. J Intel Fuzzy Syst 2(3):267–278
27. Kecman V (2000) Learning and soft computing. MIT Press, Cambridge, MA
28. Samhouri MS, Surgenor BW (2005) Surface roughness in grinding: on-line prediction with adaptive neuro-fuzzy inference system. Trans NAMRI/SME 33:57–64
29. Samanta B, Erevelles W, Omurtag Y (2008) Prediction of workpiece surface roughness using soft computing. Proc Inst Mech Eng B 222:1221–1232
30. Enemouh EU, El-Gizawy AS, Okafor AC (2001) An approach for development of damage-free drilling of carbon fibre reinforced thermosets. Int J Mach Tools and Manuf 41(12):1795–1814
31. Gilpin A (2009) Tool solutions for machining composites. Reinf Plast 53:30–33
32. Sheikh-Ahmad JY, Stewart JS, Feld H (2003) Failure characteristics of diamond-coated carbides in machining wood-based composites. Wear 255(7–12):1433–1437
33. Taylor FR (1907) On the arts of cutting metals. Trans ASME 28:31–58
34. Hocheng H, Puw HW, Huang (1993) Preliminary study on milling of unidirectional carbon fibre-reinforced plastics. Compos Manuf 4 (2):103–108
35. Shaw MC (1984) Metal cutting principles, Oxford series on advanced manufacturing. Oxford University Press, Oxford
36. Rawat S, Attia H (2009) Wear mechanisms and tool life management of WC-Co drills during dry high speed drilling of woven carbon fibre composites. Wear 267:1022–1030